JSR Publications

Available Online

J. Sci. Res. **16** (2), 613-636 (2024)

JOURNAL OF SCIENTIFIC RESEARCH

www.banglajol.info/index.php/JSR

Review Article

Search for the True Nature of Nucleus-Nucleus Potentials

M. S. Islam[1], A. S. B. Tariq[2], S. K. Joarder[2], M. A. Uddin[2], A. K. Basak[2*]

[1]Department of Physics, Hajee Mohammad Danesh Science and Technology University- Dinajpur 5200, Bangladesh

[2]Department of Physics, University of Rajshahi, Rajshahi 6205, Bangladesh

Received 22 January 2024, accepted in final revised form 7 February 2024

Abstract

A review on the research contributions from the nuclear and particle physics laboratory of Rajshahi University is presented. Special emphasis has been given to the nuclear physics research using the molecular nucleus-nucleus (NN) potentials derived from the Pauli-laden energy density functional (EDF) theory. The successes of EDF-derived non-monotonic (NM) NN potentials, compared to other familiar optical model potentials such as Woods-Saxon (WS), Squared Woods-Saxon (SWS), double folding (DF) for NN interactions, have been discussed. The phenomenal successes of NM potentials with a repulsive core have been found to suggest that the *true nature* of NN potential is NM with the Pauli-compliant EDF as its root.

Keywords: EDF; Pauli-effects; Non-monotonic potentials; DPP.

doi: https://dx.doi.org/10.3329/jsr.v16i2.71132 J. Sci. Res. **16** (2), 613-636 (2024)

1. Introduction

To interpret the origin of various nuclear species and the nature of the entire universe, the study of nucleon-nucleus (nN) [1] and nucleus-nucleus (NN) [2] interaction potentials are very essential. Reliable nN and NN potentials can only lead us to the deep learning of nuclear matters and their structures in the whole universe. However, in our article, we are concerned with the NN potentials.

The nuclear and particle physics research laboratory (NPRL) of Rajshahi University (RU) started the journey to the international arena with a presentation of a paper titled "The properties of charged hyperons and hyperfragments emitted from the interactions of 500 MeV/C negative *K* mesons with nuclear emulsion" in the 1964 Peking symposium [3]. The paper drew favourable comments from the noted Japanese Physicist Shoichi Sakata, saying the paper has thrown an important new light, which appeared in Science Chronicles and flashed the headlines of Pakistan daily newspapers. This was followed by a publication entitled "A possible decay in flight of ($^{6}Li_{\Lambda}$)*" in Lettere al Nuovo Cimento

*Corresponding author: akbasak@gmail.com

[4], a memorable one at that time. This publication was the first journal publication in all sciences of RU. Both the works were done without any computer at that time was really remarkable.

1.1. *Ph.D. degrees from NPRL before 1997*

Dr Abdus Salam Mondal, received the first Ph.D. in all sciences of RU in 1974, in the field of particle-nuclear physics using the interesting reaction products, relating the decays of *hyperfragments*, produced in the nuclear emulsion plates exposed to 3.0 GeV/c negative *K*-mesons at CERN proton synchrotron. He worked on the binding energies of hyperon-nucleus (BEHN) in nuclei. BEHN's are useful to understand the hyperon-nucleon force. The plates were received in 1959 under the auspices of Dr W. O. Lock in CERN. His thesis work produced illuminating papers [4-6].

Dr. Md. Abul Basher submitted his Ph.D. thesis in 1992 in the field of nuclear physics on the spectroscopic structure of ^{52}Cr and ^{64}Cu using, respectively, the ^{51}V (^{3}He, d) and ^{51}V (^{3}He, p) reactions at 15 MeV leading to the publications of [7,8].

In the middle of the nineties, the laboratory (Lab) braved stepping into a multi-disciplinary field like "Modeling the Influence of Climatic Factors on Rice Production in Bangladesh" submitted in 1995 by Dr. Md. Serajul Islam for his Ph.D. degree. The model is found profoundly seminal in the present scenario of immense climate change.

1.2. *Development of atomic and molecular research field in NPRL*

The Lab is the doorway to the development of 'the atomic and molecular research field" in the Physics Department of RU through the Ph.D.'s of Prof. M. Alfaz Uddin and Prof. A. K. Fazlul Haque. They submitted the Ph.D. theses, respectively, in 2004 and 2006. Both of them are now key persons of the Atomic and Molecular Physics Group, with Prof. Alfaz Uddin as the leader.

1.3. *Beginning of nuclear physics research using molecular NN potentials*

In 1997, we stepped in the examination of the molecular [synonymous with non-monotonic (NM)] potentials with a repulsive core on the NN interactions through the M.Sc. works of Abdullah Shams Bin Tariq (now Professor and co-author of this paper) and his class-fellow AFM Mizanur Rahman (now Dr. and Principal Scientific Officer at Nuclear Power Plant Project Office, Atomic Energy Commission, Dhaka). NM potential has its roots in the Pauli-laden Energy density formalism (EDF) theory of Brueckner, Coon and Dabrowski (BCD) [9].

2. Importance of Optical Potentials (OPs) and Its Components

Knowledge of the NN optical potential (OP) is a key ingredient to the estimation of cross sections (CSs) of elastic scattering and non-elastic processes including the fusion reactions, and in understanding reaction dynamics, spectroscopy of a nucleus, how heavy elements are formed, Equation of State (EoS) and its fundamental property, nuclear incompressibility *K* in astrophysics and in isotope production for medical treatment.

Optical potentials (OPs) have real part comprising nuclear and Coulomb potential, and imaginary part as the following:

$$U(R) = V_C(R) + V_N(R) + iW_I(R). \quad (1)$$

The Coulomb potential $V_C(R)$ is assumed to be due to a uniformly charged sphere of radius R_C and is given by

$$V_C(R) = \left[\frac{Z_1 Z_2 e^2}{2R_C}\right]\left[3 - \frac{R^2}{R_C^2}\right] \text{ for } R \leq R_C$$

$$= \frac{Z_1 Z_2 e^2}{2R_C} \text{ for } R > R_C \quad (2)$$

The most common forms of the imaginary potential W_I (R) used as Woods-Saxon (WS) [8], Squared Woods-Saxon (SWS) [9], and Gaussian (GS) [10] forms are the following:

Woods-Saxon (WS) form

$$W_I(R) = -W_0\left[1 + exp\left(\frac{R-R_I}{a_I}\right)\right]^{-1} + 4W_D a_D \frac{d}{dR}\left[1 + exp\left(\frac{R-R_D}{a_D}\right)\right]^{-1} \quad (3)$$

Squared Woods-Saxon (SWS) form

$$W_I(R) = -W_0\left[1 + exp\left(\frac{R-R_I}{2a_I}\right)\right]^{-2} \quad (4)$$

Gaussian (GS) form

$$W_I(R) = -W_0\, exp\left[-\left(\frac{R}{R_W}\right)^2\right] - W_S\, exp\left[-\left(\frac{R-D_S}{R_S}\right)^2\right] \quad (5)$$

In Eqs. (2.3 – 2.5) the quantities bear usual meaning.

2.1. *Classification of Optical Potentials (OPs)*

Classification of OPs is based on their real part. The real nuclear part $V_N(R)$ in Eq. (1) can be obtained in different form factors, generated through either phenomenological models or microscopic theories. The phenomenological OP is directly obtained from the analysis of elastic scattering data without a unique set of potential parameters due to discrete and continuous potential ambiguities [13-15], associated with it. The removal of potential ambiguity is also challenging. The discrete potential ambiguity can only be eliminated in the refractive angular structure at higher energies for all types of OPs, where the primary nuclear rainbow is followed by exponential type fall-off in the classically forbidden region [16, 17]. All OPs can be grouped into two categories: monotonic and non-monotonic (NM), respectively, without and with a repulsive core.

The molecular potentials derived from the BCD's EDF theory [9] are NM and shallow in terms of volume integral per nucleon pair $J_R/(A_P A_T)$, Ap and A_T being the mass numbers of the projectile and target nuclei, respectively. The familiar WS [10], SWS [11] and widely used double folding (DF) [18] potentials are monotonic and deep.

2.2. *Our motivation and forms of familiar OPs*

Our motivation is to adjudge the successes of NM potential compared to familiar OPs including the most familiar WS [10], special SWS due to Michel [11], the phenomenological version of the microscopic 'Resonating Group Method (RGM)' due to Wada and Horiuchi [19] and widely used double folding (DF) [18]. We call the special SWS due to Michel as the Michel Potential. The forms of these familiar OPs are:

Woods-Saxon (WS)

$$V_N(R) = -V_0\left[1 + exp\left(\frac{R-R_0}{a_0}\right)\right]^{-1} \tag{6}$$

Squared Woods-Saxon (SWS)

$$V_N(R) = -V_0\left[1 + exp\left(\frac{R-R_0}{2a_0}\right)\right]^{-2} \tag{7}$$

Special SWS, the phenomenological version of the microscopic 'Resonating Group Method (RGM)' due to Wada and Horiuchi [19].

$$V_N(R) = -V_0\left[1 + \alpha\, exp\left(-\left(\frac{R}{R_W}\right)^2\right)\right]\left[1 + exp\left(\frac{R-R_0}{2a_0}\right)\right]^{-2} \tag{8}$$

Here the factor in the parameter *a* is a new addition to Eq. (8) to get to the special SWS.

Double Folding (DF)

$$V_{DF}(R) = \iint \rho_A(\vec{r}_1)\rho_a(\vec{r}_2)v(\vec{r}_{12})d^3\vec{r}_1 d^3\vec{r}_2 \tag{9}$$

$V_{DF}(R)$ is the direct convolution of nucleon-nucleon (n-n) potential over the densities of projectile and target densities. Effective n-n potential in the DF calculations is density-dependent M3Y interaction, which is based on the G-matrix elements [20] having two variants M3Y-Reid using Reid n-n interaction [21] and M3Y-Paris in Paris interaction [22]. The M3Y interactions are central, independent of spin and isospin.

2.3. *EDF potentials of Brueckner, Coon and Dabrowski (BCD)*

Unlike the DF potentials, EDF-potentials are generated from the total energies of the projectile, target and the composite nucleus, formed during the collision. The total energy of each of the three nuclei is computed by folding a realistic n-n potential over the respective density distribution function (DDF). The EDF potential *V(R)* [9, 12, 23] including the Coulomb potential $V_C(R)$ between the projectile and the target at a separation distance of *R* is given by

$$V(R) = E[\rho(\boldsymbol{r}, R)] - E[\rho_P(\boldsymbol{r}, R = \infty)] - E[\rho_T(\boldsymbol{r}, R = \infty)] \tag{10}$$

Here ρ is the DDF of the composite system, and ρ_P and ρ_T are, respectively, the DDFs for the projectile and the target at R=∞. In the sudden or frozen approximation, the DDF of the composite system is given by,

$$\rho(\boldsymbol{r}) = \rho_P(\boldsymbol{r}) + \rho_T(\boldsymbol{r}). \tag{11}$$

In the EDF theory, the energy of a nucleus for a given density distribution $\rho(r)$ is expressed [9, 24] as

$$E = \int \varepsilon[\rho(\boldsymbol{r})]\mathrm{d}^3\boldsymbol{r}. \tag{12}$$

Here, $\varepsilon[\rho(\mathbf{r})]$, the energy density is given by

$$\varepsilon[\rho(\boldsymbol{r})] = 0.3\left(\frac{\hbar}{2M}\right)\left(\frac{3\pi^2}{2}\right)^{\frac{2}{3}}[1-\xi)^{\frac{5}{3}} + (1+\xi)^{\frac{5}{3}}] \times \rho^{\frac{5}{3}} + v(\rho,\xi)\rho$$

$$+\frac{e}{2}\Phi_C(\boldsymbol{r})\rho_p - 0.739e^2\rho_p^{4/3} + \left(\frac{\hbar^2}{8M}\right)\eta(\nabla_\rho)^2. \tag{13}$$

In Eq. (13), *M* is the nucleon mass and $\xi = (N-Z)/A$ is the neutron excess parameter. The first term in Eq. (13) arises from the nucleon kinetic energy in nuclear matter. The second term, the nucleonic mean field $v(\rho, \xi)$, is determined from the Gammel-Christian-Thaler (GCT) n-n potential [25] in the Brueckner-Hartree-Fock (BHF) theory. The GCT potential includes central, spin-orbit and tensor parts of the realistic NN potential**,** *which is able to describe all the properties of deuteron and the NN scattering data up to the pion threshold (~ 137 MeV).* In the BHF theory the mean field relates the matrix elements of the n-n potential [9] to those of the scattering operator with full consideration of the Pauli principle among the nucleons of the same type in the nuclear and nucleonic matter approximations, i.e., using the plane wave for nucleonic wave functions. The third and fourth terms represent, respectively, the Coulomb energy and its correction due to the Pauli principle among protons [12,23,24]. The last term incorporates the inhomogeneity correction [23,24] to the kinetic energy due to the finite size and correlation effect among nucleons, not included in the mean-field calculation.

BCD's EDF [9,12] provides the Equation of State (EoS) i.e. The binding energy per nucleon versus density curve for cold nuclear matter with the nuclear incompressibility value K = 188 MeV at the saturation density, defined [9,12] through the curvature of $B(\rho,\xi)$ at the saturation density ρ_0 as**,**

$$K = 9\rho_0\left[\frac{d^2B}{d\rho^2}\right]_{\rho=\rho_0} \tag{14}$$

Harder EoSs for higher *K*-values with identical features at lower densities up to the saturation have been simulated [12].

2.4. *Non-monotonic (NM) potential form*

The EDF derived non-monotonic (NM) potentials are usually parameterized [12] by the following form:

$$V_{NM}(R) = -V_0\left[1 + exp\left(\frac{R-R_0}{a_0}\right)\right]^{-1} + V_1\, exp\left[-\left(\frac{R-D_1}{R_1}\right)^2\right] \tag{15}$$

This serves as the NM real part of OP. The associated empirical imaginary part is taken with the Gaussian form-factors given in Eq. (5).

3. Successes of NM Potentials

3.1. *Success 1*

The impact of different EoSs on the nuclear potentials $V_N(R)$ for typical ^{16}O-^{16}O interaction potential shows that at smaller radial distances (at the nuclear interior of the composite nucleus) the repulsive potential increases with K as shown in Fig. 1. This leads to the decreasing volume integral per pair $J_R/256$ with increasing K-values as depicted in Fig. 2. The legend in this plot showing K-dependence of $J_R/256$-values can be used as calibration for finding the K-value for a symmetric homogeneous nuclear medium from analyzing the cross section (CS) data of the ^{16}O-^{16}O elastic scattering at different energies. The excitation energy E_X of the composite nucleus ^{32}S is related to the incident laboratory energy E_{lab} by $E_X = 16.54 + E_{lab}/2$ with 16.54 MeV as the breakup threshold energy of ^{32}S.

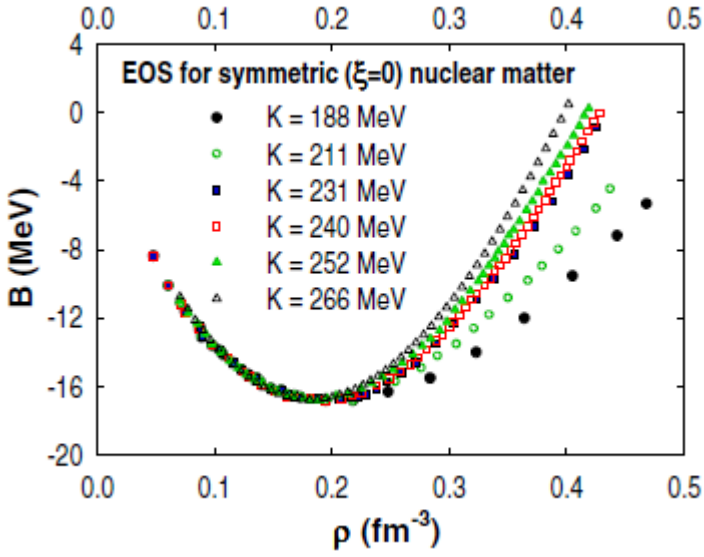

Fig. 1. EoSs for six K-values at the saturation point for symmetric infinite nuclear matter. Illustration is taken from [12].

The energy variation of $J_R/256$ fitting the experimental CS data versus E_X plot is regressed by a power function $80.9 - 0.0003E_X^{2.42}$ as displayed in Fig. 3. The regression curve gives the extrapolated value of $J_R/256$ = 80.9±1.1 MeV.fm^3 at E_X = 0 MeV of the composite nucleus. From the calibration legend in Fig. 2, this $J_R/256$-value yields directly K=222±5 MeV for an infinite cold nuclear matter as in neutron stars. [The error-bar includes the uncertainties in the extracted $J_R/256$ values from fitting the CS data, curve fitting and extrapolation]. Detailed procedure can be obtained in our paper [12]. Our K=222±5 MeV compares much better than the DF value of K= 230-260 MeV [17].

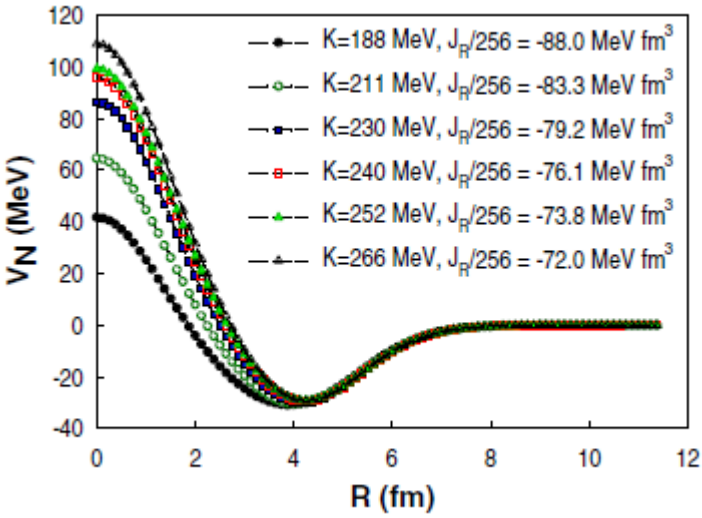

Fig. 2. *K* dependence of the EDF-generated ^{16}O-^{16}O nuclear potential with the volume integral $J_R/256$ values in the legend. The latter serves as the calibration of *K*. Illustration is taken from [12].

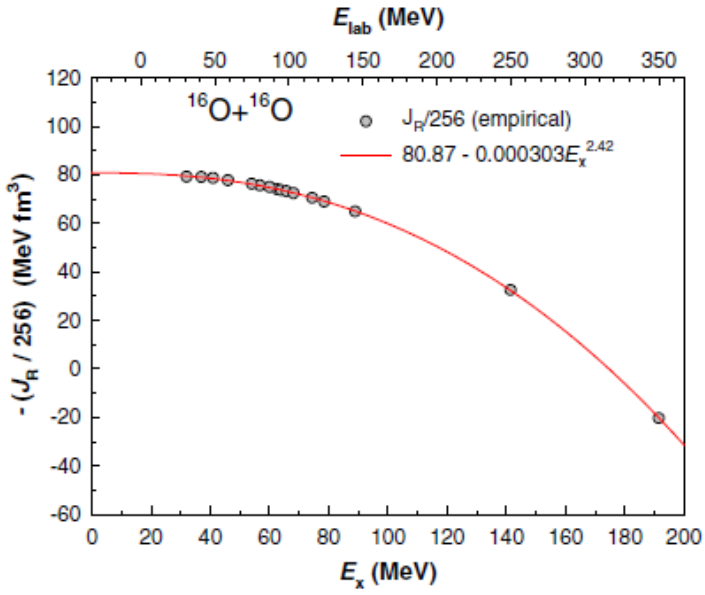

Fig. 3. Variation of $J_R/256$ with E_X and the regression curve through the derived points in open circle. Illustration is taken from [12].

3.2. *Success 2*

Let us now come to compare the predicted results of α-elastic and the inelastic scattering on ^{28}Si obtained, respectively, by Tariq *et al*. [26] and Basak *et al*. [27] using different potentials including the NM (molecular) and Michel (special SWS) potentials in Eq (8). The results of the elastic scattering [26] are shown in Fig. 4 and those of inelastic scattering [27] are depicted in Fig. 5.

One can see in Fig. 4, the quality of fits to the elastic data for the NM and Michel potentials is found adequately similar. The WS potentials are inadequate to fit the data at large angles. In the case of the inelastic scattering to the 1.76 MeV (2+) and 4.61 MeV (4+) states of ^{28}Si, the NM potential is found somewhat better than the Michel one (see Fig. 5).

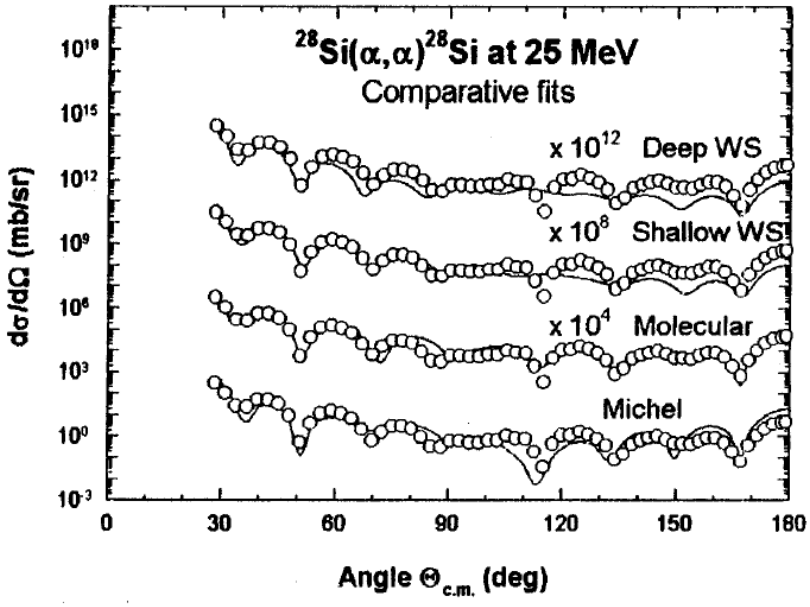

Fig. 4. Fits for the α-^{28}Si elastic scattering data at 25 MeV with shallow WS, deep WS, molecular (NM), and Michel (special SWS) potentials. The inadequacy of the WS potentials is evident at large angles. Illustration is taken from [26].

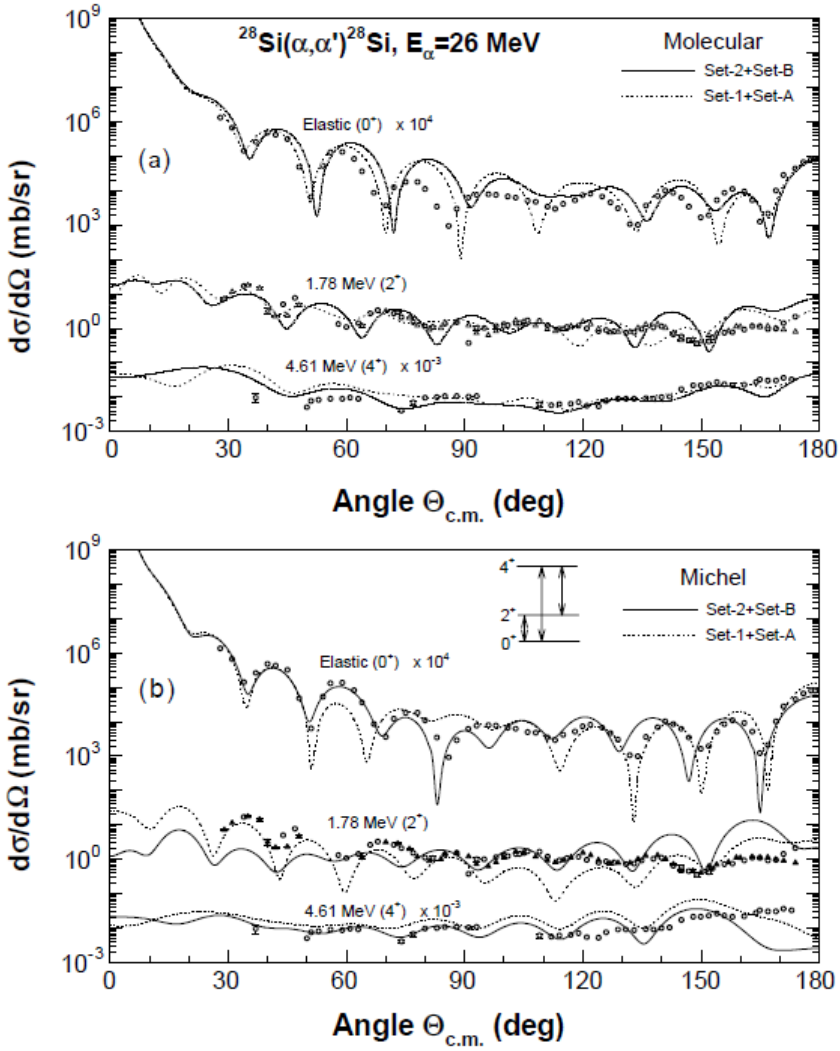

Fig. 5. Comparison of the predictions from the coupled channel (CC) microscopic calculations for the elastic and inelastic alpha-scattering to the 2^+ and 4^+ states of ^{28}Si with the angular distribution data. The solid curves are the predictions with (a) Molecular and (b) Michel potentials in the alpha channel. The coupling scheme is shown in (b). The open circles and triangles are the experimental points. Illustration is taken from [27].

3.3. *Success 3*

Let us now compare the performances of the molecular (NM), Michel (special SWS), shallow WS optical and deep WS optical potentials for the ^{28}Si (α, p)^{31}P reaction populating the ground $(1/2)^+$, 1.27 MeV $(3/2^+)$ and 2.23 MeV $(5/2)^+$ states of ^{31}P in the framework of DWBA [28]. Here one can see that Michel and deep optical WS potentials are performing poor, molecular NM doing the best and shallow optical WS, fairly well

excepting at the large angles as shown in Fig. 6. The predicted results from the Michel and deep WS are at least 3 orders of magnitude down compared to the experimental data of Jankowski *et al.* [29].

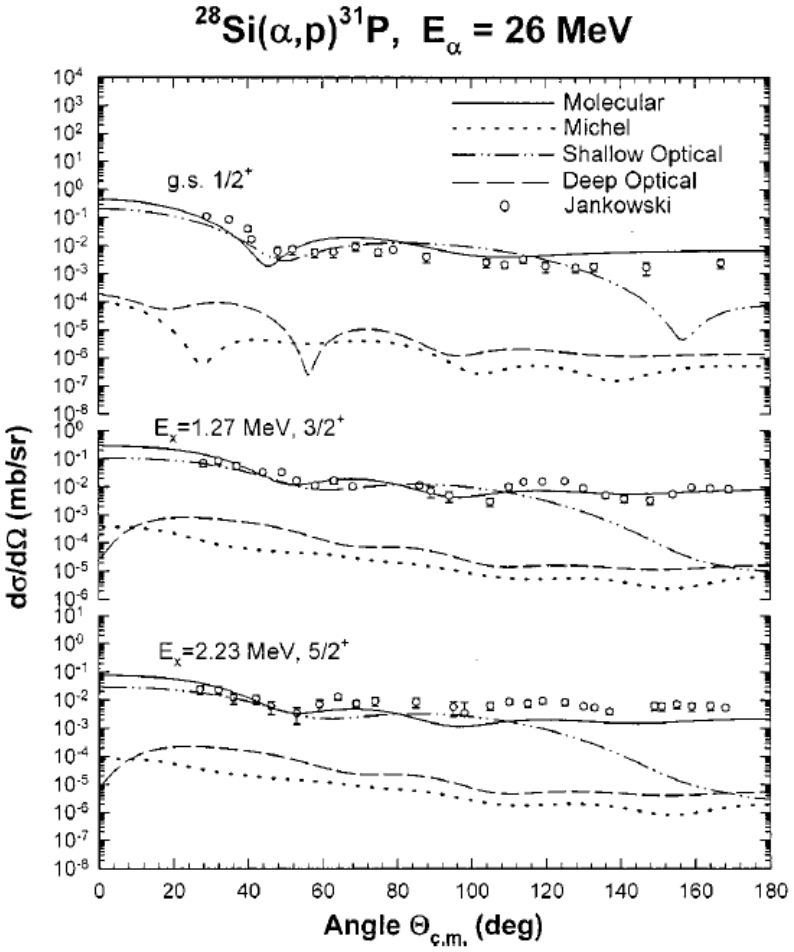

Fig. 6. Calculated angular distributions in zero-range DWBA for the (α, *p*) reaction using four potentials noted in the upper right-hand corner. The experimental data [29] marked as open circles. Illustration is taken from [28].

3.4. *Success 4*

Now let us compare the performance of NM (top frame) and DF (bottom frame) potentials in α-elastic scattering by ^{90}Zr. The NM illustration is from our paper [24] shown in Fig.7. DF results are from [30] shown in Fig. 8. Fits to data using DF potentials below $E_{lab} \leq 59.1$ MeV do not exist. DF has limitation at lower energies and needs renormalization of its potentials to fit data. Our fit at 40 MeV is excellent. And our fits at 99.5 and 119 MeV are better than DF's.

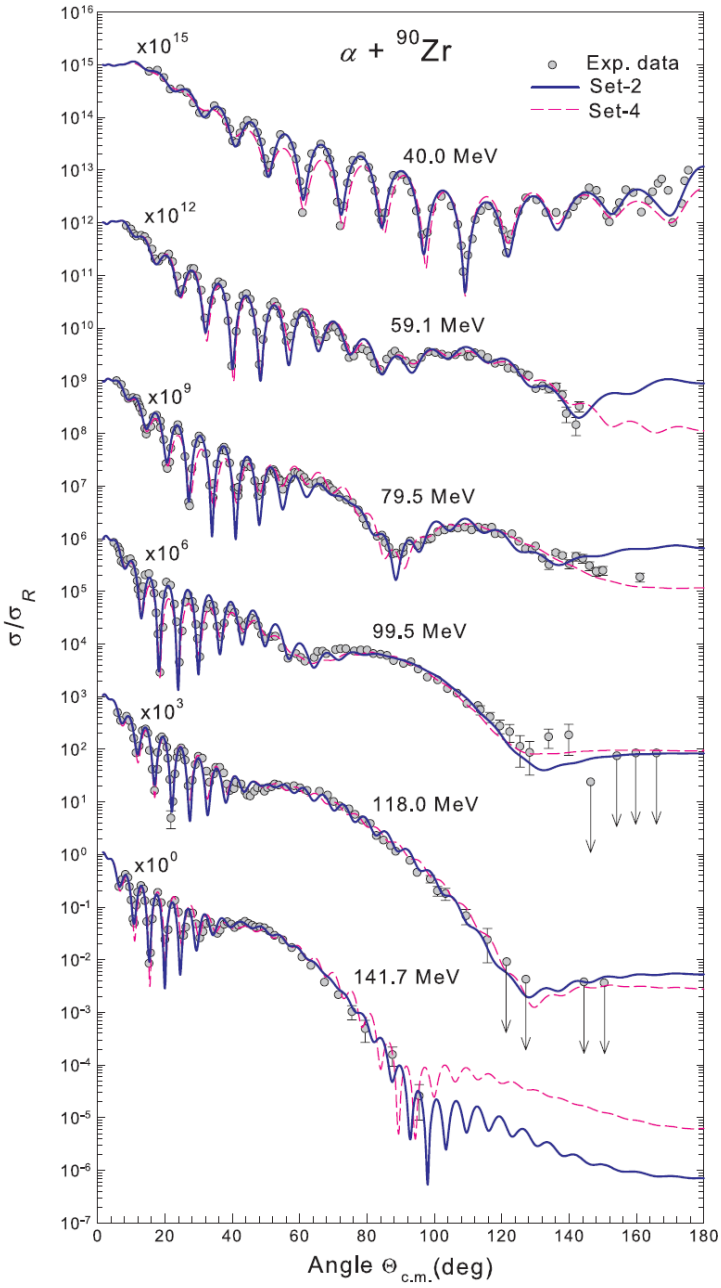

Fig. 7. Non-monotonic (NM) description of α-^{90}Zr elastic scattering at 3 energy points in the range E_{lab} = 40 - 141.7 MeV. Illustration is taken from [24].

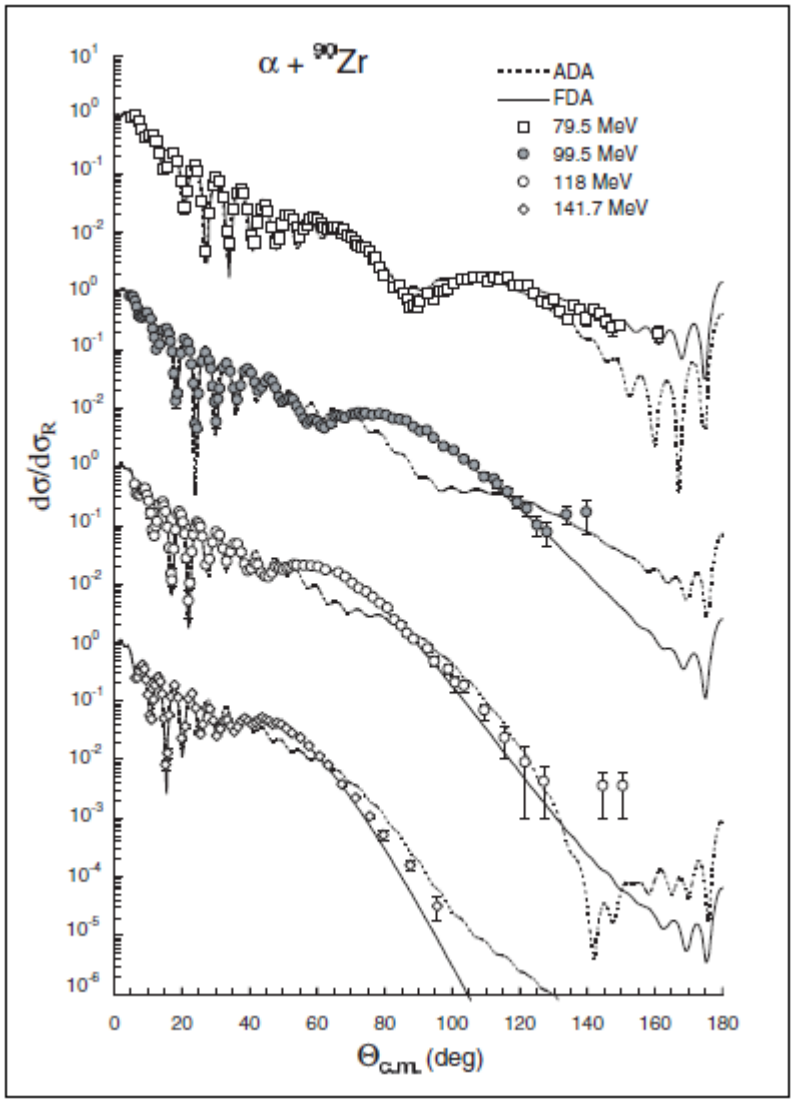

Fig. 8. Double folding (DF) description of α-^{90}Zr elastic scattering at 79.5 to 141.7 MeV. Illustration is taken from [30].

3.5. *Success 5*

^{6,7}Li being primordial nuclei are important for our understanding of stellar nucleosynthesis. Elastic scattering of ^{6,7}Li is challenging to describe the experimentally observed the large and the opposite signs of vector analyzing power (VAP) iT_{11} data for the ^{6}Li and ^{7}Li elastic scattering [31]. Moreover, as noted in [32], the DF potentials need a large renormalization factor of N_R = 0.5-0.6 [32] in the simple OM to reproduce the CS data and a failure completely to explain the opposite signs of iT_{11} for the ^{6,7}Li elastic

scattering. NM potentials for ^{6,7}Li –nucleus elastic scattering [31] without any adjustment to the EDF-generated potentials are found to describe the experimental CS and iT_{11} data of elastic scattering on ^{12}C, ^{26}Mg, ^{58}Ni and ^{120}Sn in simple optical model (OM). The opposite signs of iT_{11} data for ^{6}Li and ^{7}Li elastic scattering on the same target and at similar energies could be reproduced using EDF potentials (see Figs. 9-10). *With our reported results* [31] *a long-standing puzzle could be settled.*

To justify our success, we look to the single folding calculations of Nishioka *et al*. [33] for ^{6,7}Li elastic scattering on ^{58}Ni. DF calculations provide similar information. The work in [33] made predictions for CS and iT_{11} in coupled-channels (CC) for variable number of channels for clarity in dynamics. The results presented in Figs. 11-12 are displayed in short-dashed lines for single-channel (optical model); in solid lines for two-channel and dashed lines for four channel calculations. Fits get improved with increasing channel number. However, fits to the CS data are not as good as our OM calculations shown in Fig. 10.

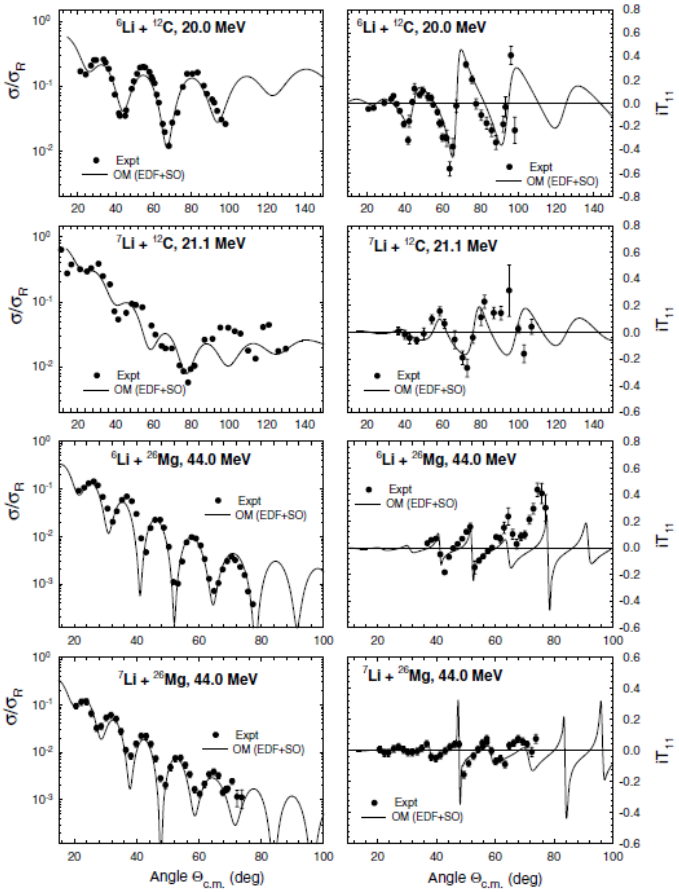

Fig. 9. The OM predictions of ^{6,7}Li elastic scattering by ^{12}C and ^{26}Mg using the EDF generated real central potentials. Illustration is taken from [31].

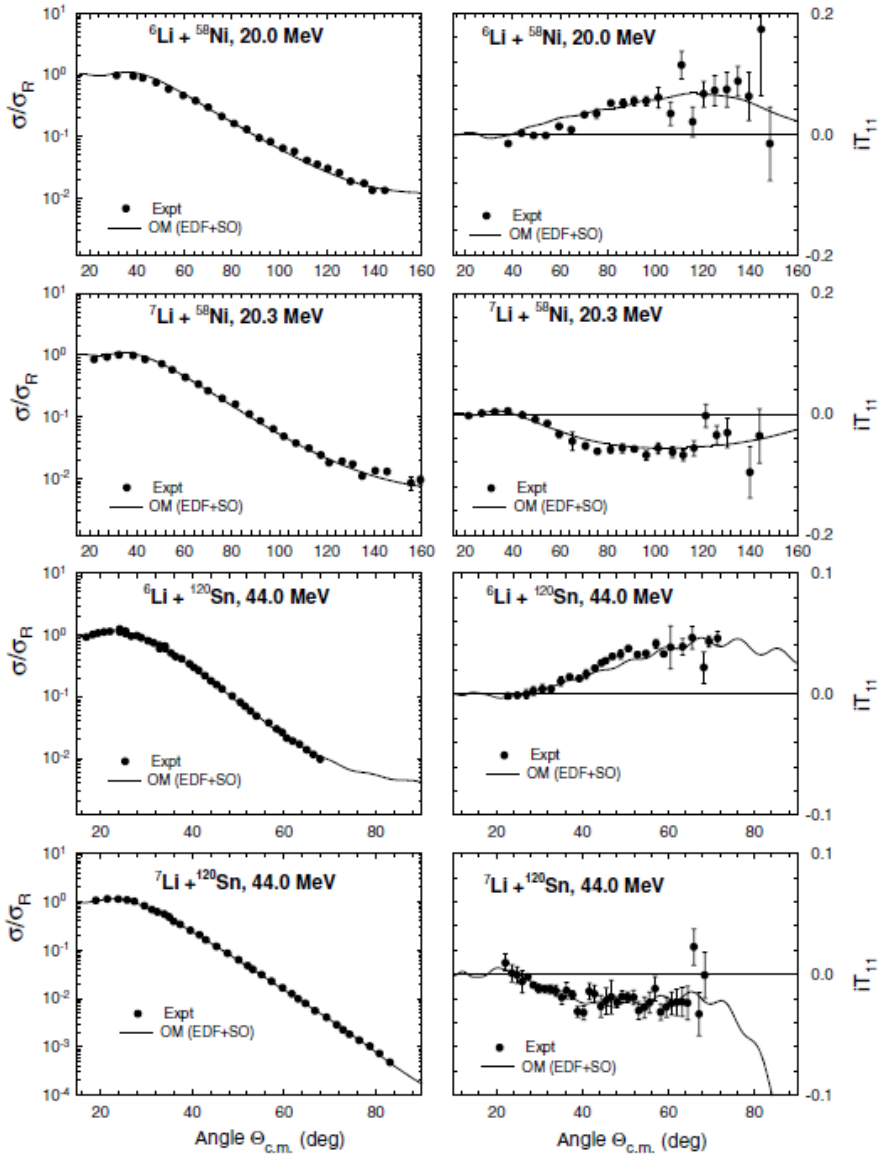

Fig. 10. Same as Fig. 9 for ^{6,7}Li elastic scattering on ^{58}Ni and ^{120}Sn. Illustration is taken from [31].

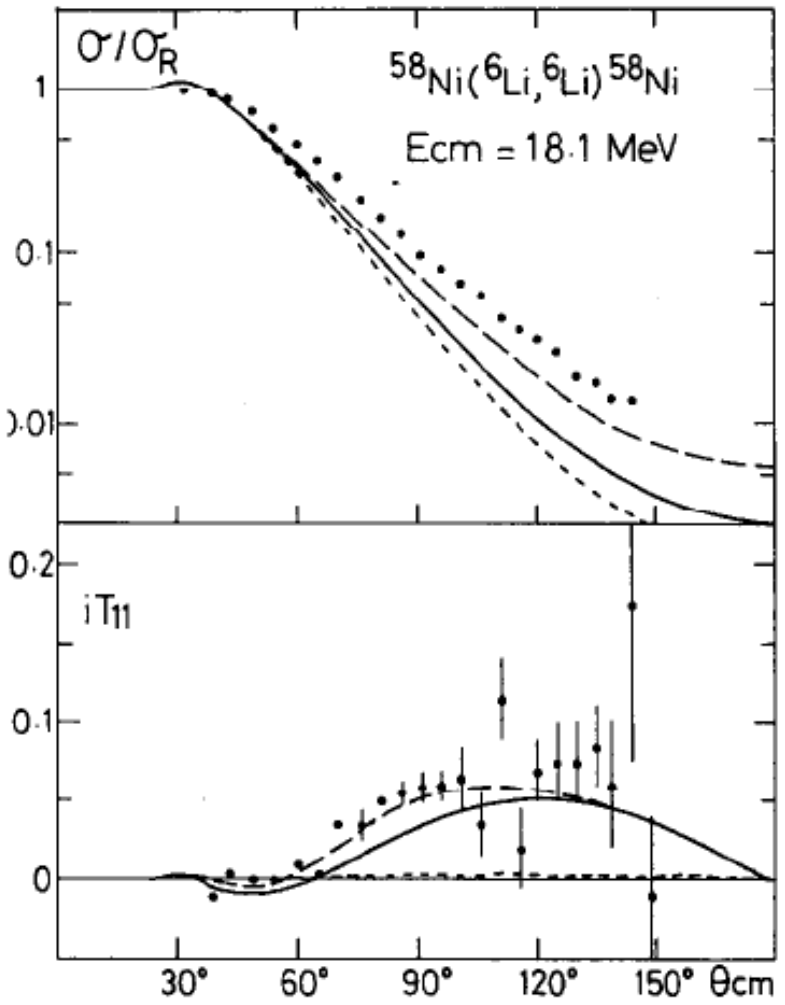

Fig. 11. Results of CC calculations on the ^{6}Li +^{58}Ni elastic scattering for the CS and vector analyzing power iT_{11} at E_{cm}=18.1 MeV (E_{lab}= 20 MeV). The short dashed, solid and dashed curves are the results of one-channel, two-channel, and four channel calculations, respectively. Illustration is taken from [33].

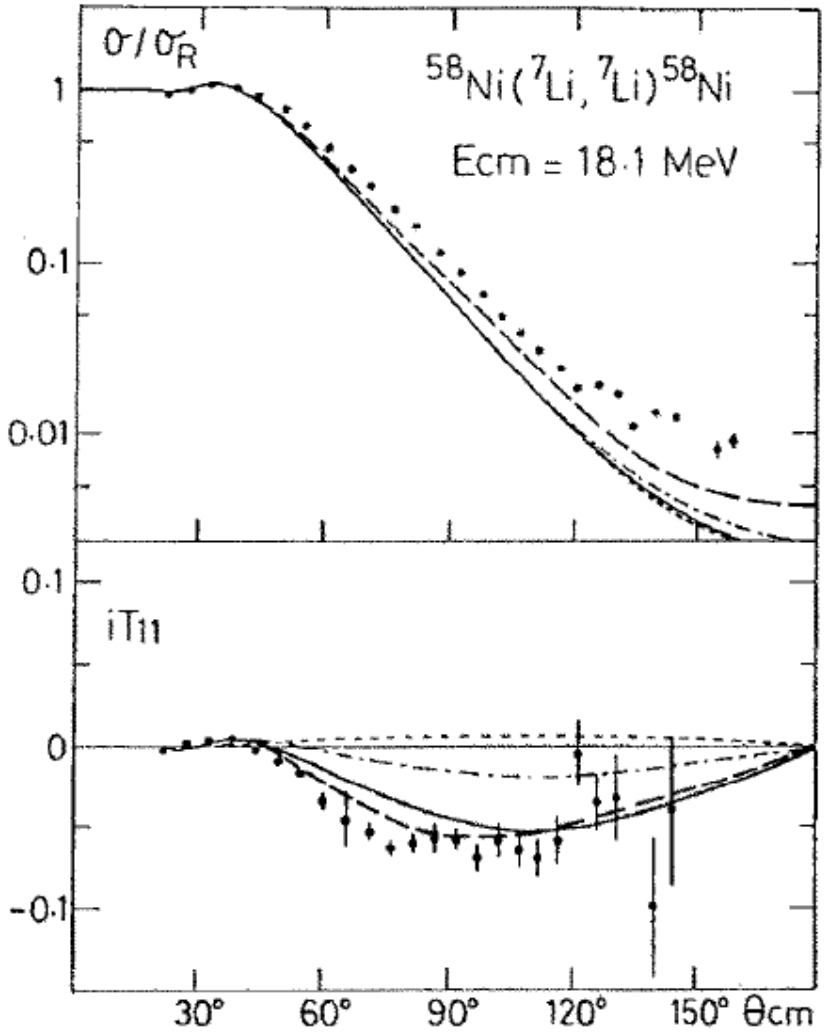

Fig. 12. Same as Fig. 11 but for ^{7}Li+^{58}Ni elastic scattering. Illustration is taken from [33].

3.6. *Success 6*

Now we compare our NM results from [34] presented in Fig. 13 for CS, vector analyzing power iT_{11} and tensor analyzing powers (TAP) T_{20}, T_{21} and T_{22} of ^{6}Li +^{12}C elastic scattering at E_{lab}= 30 MeV with those of [35] in Fig. 14. Kerr *et al*. [35] used six-channel CC calculations using the DF potentials and we did in simple OM using the NM potentials. In the overall picture, our results seem to be better (see iT_{11} and T_{22} predictions in red in Fig. 13 compared to Kerr *et al*. [35].

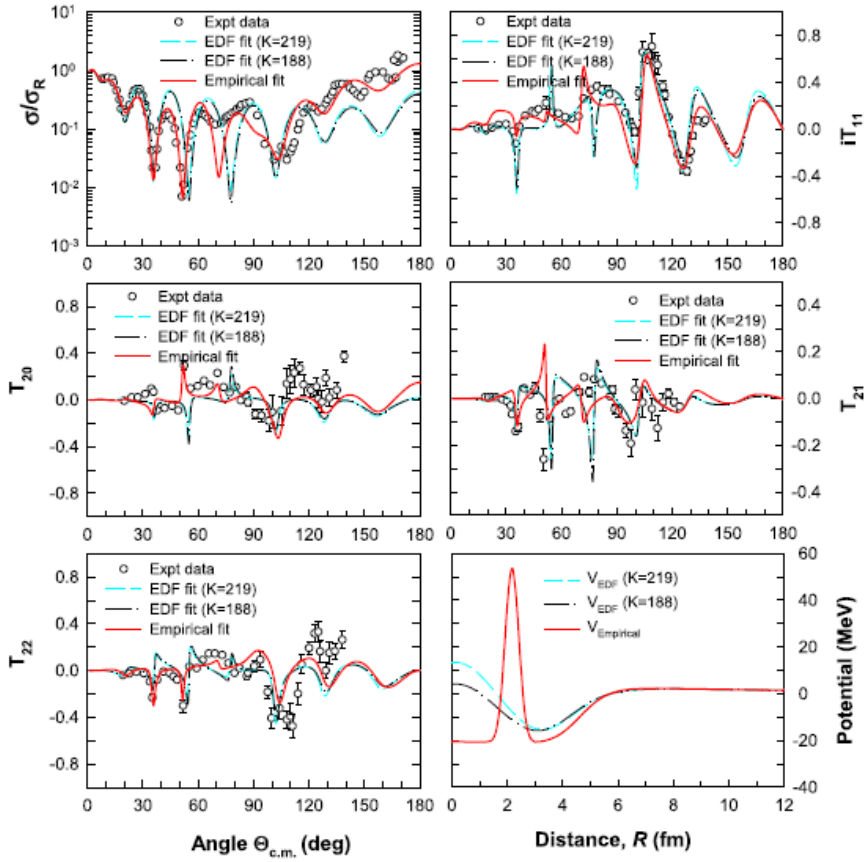

Fig. 13. NM description of CS, iT_{11}, T_{20}, T_{21} and T_{22} for the ^{6}Li+^{12}C elastic scattering at 30 MeV. Illustration is taken from [34].

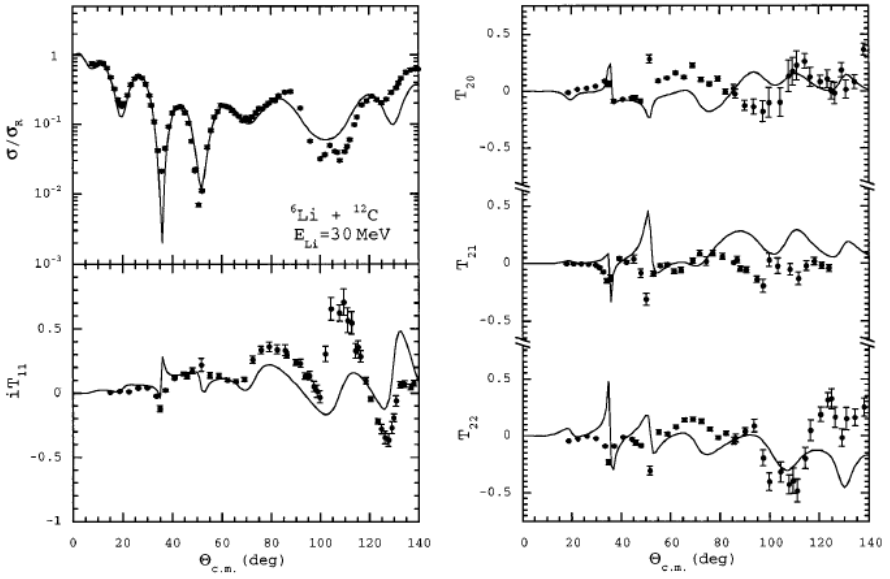

Fig. 14. Same as in Fig. 13 in 6-channel CC calculations using the DF potentials. Illustration is taken from [35].

3.7. *Success 7*

A potential family is marked by a smooth energy-variation of volume integral $J_R/(A_pA_T)$ of projectile-target (p-T) potential. Potential families are the consequence of discrete ambiguity at the same energy in the p-T potentials fitting an experimental CS data set having different $J_R/(A_pA_T)$ values (see Figs. 15-16). At low incident energies, nucleus-nucleus (NN) interaction reveals a set of potential families. ^{16}O-^{16}O potential families in Fig. 15 are taken from our paper [36] and ^{12}C-^{12}C potential families in Fig. 16 are from our paper [37]. Our work confirms the Goldberg criterion [16] that "at sufficiently high energies, where the primary rainbow maximum is followed by an 'exponential-type falloff' in the classical shadow region of the angular distribution, discrete potential ambiguities are eliminated for a deep potential". In both of our papers [36,37] it is demonstrated that the Goldberg criterion works also for shallow NM potentials. Thus, our finding suggests that the requirement of a deep attractive real part of the nuclear potential as asserted in the Goldberg criterion is 'non-essential'.

Moreover, the Goldberg criterion does not suggest the energy for the first appearance of the primary rainbow which is important for the identification of the order of the Airy minima in the refractive scattering structure. Based on the findings from our papers [36,37], two assertions have been made to glorify the Goldberg criterion: (*i*) The first conjecture relates to the first appearance of the primary nuclear rainbow which occurs at the energy of convergence of the potential families (with the discrete ambiguities) and (*ii*) The second conjecture may be stated as 'with the elimination of discrete ambiguity at higher energies the volume integral (A_pA_T)-values belong to a unique potential family'. In case of the NM potentials, derived from the Pauli-embodied EDF of BCD, the unique

family is the EDF-family or set-1 family in our notation (see Figs. 15-16). Behaviour of NM potentials at low energies shows that around the Coulomb barrier valley (CBV) in the region of Coulomb barrier, with the onset of Coulomb inelastic scattering the dispersion effect [38] increases the $J_R/(A_PA_T)$ values (see the insets of Figs. 15-16). This is also referred to as "threshold anomaly" near the Coulomb barrier. The flat behaviour in the energy-variation of the volume integral $J_R/(A_PA_T)$ outside CBV offers a reliable nucleus-nucleus potential for the real part of OP in estimating the fusion cross section (FCS). This has been accomplished for FCS of $^{16}O+^{16}O$ in our paper [36].

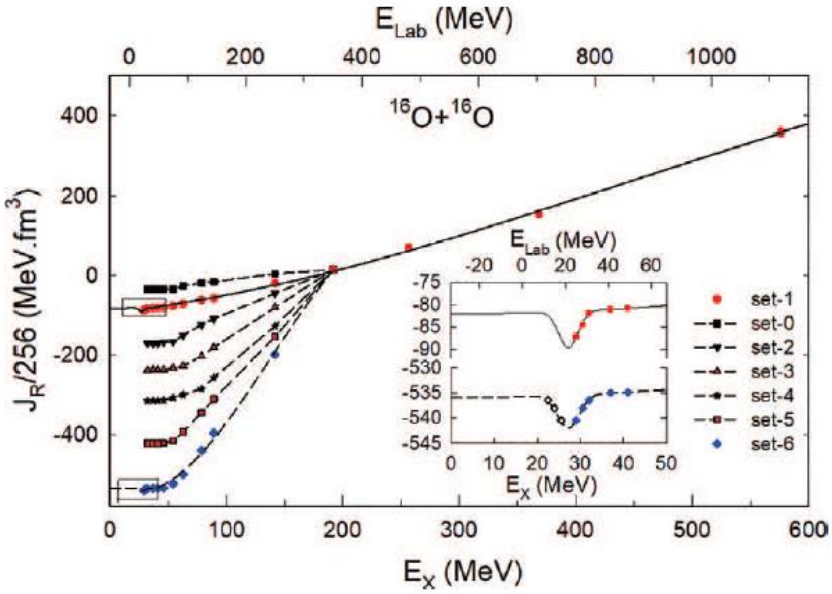

Fig. 15. Potential families at low energies E_{lab} or E_X =16.54 + E_{lab}/2 vs J_R/256 plots for set-0, set-1, set-2, set-3, set-4, set-5 and set-6 with the regression lines through the set-1 and set-6 families in the energy range 25-1120 MeV. Illustration is taken from [36].

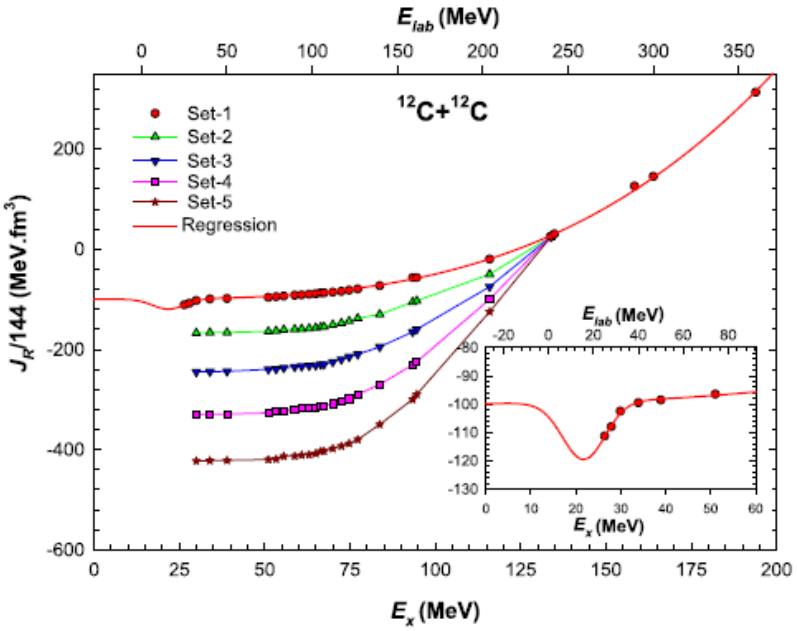

Fig. 16. Same as Fig. 15 with regression curve through the set 1 for $^{12}C+^{12}C$ elastic scattering. Illustration is taken from [37].

4. Reasons for Success with the NM Potentials

One may be tempted to know why NM potentials originating from EDF of BCD have enjoyed so many successes. Reasons for successes are ascribed to the following:

(i) The Pauli principle is properly incorporated in BCD's EDF theory, we use.

(ii) It has the scope of examining the binding energies (BEs) of the interacting nuclei in selecting their densities of the projectile and target nuclei.

(iii) The most important point is that the nucleon-nucleon (n-n) potential of GCT [25], used in BCD's EDF, is spin- and tensor-dependent, apart from the central part. The GCT n-n potential can describe all properties of deuteron and the n-p scattering up to the pion threshold.

The spin- and tensor-dependent n-n interaction can stimulate the dynamic polarization potential (DPP) [39] elaborately as we can see later on. In the DF-potential generation, the applied G-matrix of n-n interaction M3Y is only central and independent of spin- and tensor- potential. However, the CC calculations with the DF potentials can trigger spin- and tensor- effects through DPP as we have seen in the description of the VAP data for the $^{6,7}Li$-^{58}Ni elastic scattering by Nishioka *et al.* [33] (see Figs. 11-12) and vector and tensor analyzing power data for the ^{6}Li-^{12}C scattering by Kerr *et al.* [35] (see Fig. 14).

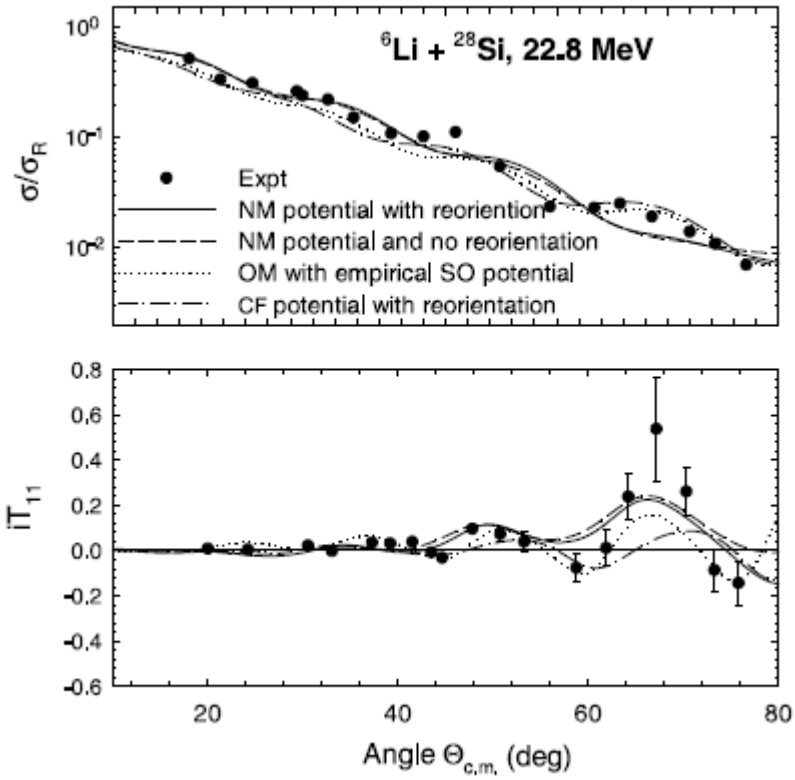

Fig. 17. Experimental σ/σ_R and iT_{11} data for the ^{6}Li-^{28}Si elastic scattering at 22.8 MeV are compared with the predictions from the four channel CC calculations. Solid lines representing the calculations without the addition of static spin-orbit potential describes the CS and iT_{11} data fairly well, better than other calculations that follows. Dotted lines here represent the one channel OM calculations with EDF generated NM real part of the ^{6}Li potentials, and empirical imaginary and static SO parts. Dash-dotted lines are the results of calculations using the cluster folding (CF) ^{6}Li potential with reorientations and without any SO potentials. Illustration is taken from [42].

DPP produces repulsive potential for renormalization of interaction potentials needed to describe the CS data. DPP also triggers the dynamic spin-dependent potentials to generate the spin-dependent effects like analyzing powers. It is to be noted here that the DPP effect in CC calculations using DF potentials may not be enough at lower energies and as such the DF potential even with CC calculations does not play well at lower energies. For example, the CC calculations with DF potentials did not fit well for the ^{6,7}Li-^{58}Ni elastic CS data at E_{cm}= 18.1 MeV (E_{lab} = 20 MeV) (see Figs. 11-12) and also the iT_{11} and T_{22} data for the ^{6}Li-^{12}C elastic scattering at 30 MeV could not be adequately described (Fig. 14). The need to add a repulsive core was revealed through the successes in describing sub-barrier fusion in CC calculations using DF potentials in the works of [40, 41]. However, at higher energies DF potentials work better through an energy dependent

factor, empirically built into it. Our work in [42] on ^{6}Li+^{28}Si elastic scattering at 22.8 MeV have demonstrated that the use of only central NM potential in CC calculation can generate adequate spin-dependent effect through DPP to account for both the CS and VAP (iT_{11}) data without the necessity of renormalization and an additional static spin–orbit (SO) potentials shown in Fig. 17.

5. Conclusion

The derived NM potentials from EDF do not have any energy-dependence built into it, so the EDF potential is strictly valid for the zero-excitation energy, E_X= 0.0 MeV, of the composite nucleus and works well up to tens of MeV. At higher excitation energies, the potential parameters are to be adjusted empirically to cope with the reduced cross sections due to reduced interaction time between the projectile and target. However, the phenomenal successes of the NM potentials suggest that the NM potential with a ***repulsive core is the "true nature" of nucleus-nucleus interactions*** with the Pauli-laden EDF as its "gateway". Successes attained with our NM potentials from EDF up to tens of MeV excel those from other existing models including widely used DF. We are now working on the ^{16}O+^{16}O fusion at the sub-Coulomb energies which is of astrophysical importance and play an important role in stellar evolution and supernovae explosions.

Acknowledgment

The authors wish to thank I. J. Thompson for his code FRESCO.

References

1. W. H. Dickhoff and R. J. Charity, Prog. Particle Nucl. Phys. **105**, 252 (2019). https://doi.org/10.1016/j.ppnp.2018.11.002
2. M. E. Brandan and G. R. Satchler and W. G. Love, Phys. Rep. **55**, 183 (1979). https://doi.org/10.1016/0370-1573(79)90081-4
3. A. Husain, A. K. Basak, G. S. Islam, M. Rahman, K. Banu, and M. Haque, Proc. Peking Sci. Symp. Gen. **147**, 1 (1964).
4. A. S. Mondal, A. K. Basak, M. M. Kasim, and A. Husain, Lettere al Nuovo Cimento **5**, 1057 (1972). https://doi.org/10.1007/BF02789709
5. A. S. Mondal, A. K. Basak, M. M. Kasim, and A. Husain, Nuovo Cimento **28**, 42 (1975). https://doi.org/10.1007/BF02730395
6. A. S. Mondal, A. K. Basak, M. M. Kasim, and A. Husain, Nuovo Cimento **54A**, 333 (1979). https://doi.org/10.1007/BF02770008
7. M. A. Basher, H. R. Siddique, A. Husain, A. K. Basak, and H. M. SenGupta, Phys. Rev. C **45**, ID 1575 (1992). https://doi.org/10.1103/PhysRevC.45.1575
8. A. K. Basak, M. A. Basher, A. S. Mondal, M. A. Uddin, S. Bhattacharjee et al., Phys. Rev. C **56**, ID 1983 (1997). https://doi.org/10.1103/PhysRevC.56.1983
9. K. A. Brueckner, S. A. Coon, and J. Dabrowski, Phys. Rev. **168**, ID 1184 (1968). https://doi.org/10.1103/PhysRev.168.1184
10. A. Nadasen, M. McMaster, M. Fingal, J. Tavormina, P. Schwandt et al., Phys. Rev. C **39,** ID 536 (1989). https://doi.org/10.1103/PhysRevC.39.536
11. F. Michel, J. Albinski, P. Belery, Th. Delbar, Gh. Grégoire et al., Phys. Rev. C **28**, ID 1904 (1983). https://doi.org/10.1103/PhysRevC.28.1904
12. S. Hossain, A. S. B. Tariq, A. Nilima, M. S. Islam, R. Majumder et al., Phys. Rev. C **91**, ID 064613 (2015). https://doi.org/10.1103/PhysRevC.91.064613

13. P. Mohr, T. Rauscher, H. Oberhummer, Z. Máté, Zs. Fülöp et al., Phys. Rev. C **55**, ID 1523 (1997). https://doi.org/10.1103/PhysRevC.55.1523
14. M. S. Islam, R. A. Ramon, M. M. Rahman, R. Majumder, M. A. Sayed et al., J. Phys. G: Nucl. Part. Phys. **48**, 075109 (2021). https://doi.org/10.1088/1361-6471/abd88e
15. G. R. Satchler et. al., Direct Nuclear Reactions (United Kingdom: Clarendon Press, 1983).
16. D. A. Goldberg, S. M. Smith, H. G. Pugh, P. G. Roos, and N. S. Wall, Phys. Rev. C **7**, 1938 (1973). https://doi.org/10.1103/PhysRevLett.29.500
17. D. T. Khoa, W. von Oertzen, H. G. Bohlen, and S Ohkubo, J. Phys. G: Nucl. Part. Phys. **34**, R111 (2007). https://doi.org/10.1088/0954-3899/34/3/R01
18. G. R. Satchler and W. G. Love, Phys. Rep. **55**, 183 (1979). https://doi.org/10.1016/0370-1573(79)90081-4
19. T. Wada and H. Horiuchi, Phys. Rev. Lett. **58**, ID 2190 (1987). https://doi.org/10.1103/PhysRevLett.58.2190
20. G. Bertsch, J. Borysowicz, H. McManus, and W. G. Love, Nucl. Phys. A **284**, 399 (1977). https://doi.org/10.1016/0375-9474(77)90392-X
21. R. Reid, Ann. Phys. (NY) **50**, 411 (1968). https://doi.org/10.1016/0003-4916(68)90126-7
22. M. Lacombe, B. Loiseau, J. M. Richard, and R. V. Mau, Phys. Rev. C **21**, ID 861 (1980). https://doi.org/10.1103/PhysRevC.21.861
23. K. A. Brueckner, J. R. Buchler, S. Jorna, and R. J. Lombard, Phys. Rev. **171**, ID 1188 (1968). https://doi.org/10.1103/PhysRev.171.1188
24. S. Hossain, M. Billah, M. M. B. Azad, F. Parvin, M. N. A. Abdullah et al., J. Phys. G 40, ID 105109 (2013). https://doi.org/10.1088/0954-3899/40/10/105109
25. K. A. Brueckner and J. L. Gammel, Phys. Rev. **109**, ID 1023 (1958). https://doi.org/10.1103/PhysRev.109.1023
26. A. S. B. Tariq, A. F. M. M. Rahman, S. K. Das, A. S. Mondal, M. A. Uddin et al., Phys. Rev. C **59**, ID 2558 (1999) https://doi.org/10.1103/PhysRevC.59.2558
27. A. K. Basak, M. N. A. Abdullah, A. S. B. Tariq, S. K. Das, A. F. M. M. Rahman et al., Eur. Phys. J. **A12**, 387 (2001). https://doi.org/10.1007/s10050-001-8662-4
28. S. K. Das, A. K. Basak, K. Banu, A. S. Mondal, A. S. B. Tariq et al., Phys. Rev. C **62**, ID 054606 (2000). https://doi.org/10.1103/PhysRevC.62.054606
29. K. Jankowski, A. Grzeszczuk, M. Siemaszko, A. Surowiec, W. Zipper et al., Nucl. Phys. A **426**, 1 (1984). https://doi.org/10.1016/0375-9474(84)90062-9
30. D. T. Khoa, Phys. Rev. C **63**, ID 034007 (2004). https://doi.org/10.1103/PhysRevC.63.034007
31. A. K. Basak, M. N. A. Abdullah, A. S. B. Tariq, S. K. Das, A. F. M. M. Rahman et al., Euro phys. Lett. **94**, 62002 (2011). https://doi.org/10.1007/s10050-001-8662-4
32. A. Pakou, Phys. Rev. C, **78**, ID 067601 (2008) https://doi.org/10.1103/PhysRevC.78.067601
33. H. Nishioka, J. A. Tostevin, R. C. Johnson, and K.-I. Kubo, Nucl. Phys. A **415**, 230 (1984). https://doi.org/10.1016/0375-9474(84)90622-5
34. A. Nilima, S. Hossain, M. M. B. Azad, M. M. Billah, A. S. B. Tariq, and A. K. Basak, J. Phys. G **47**, 085102 (2020). https://doi.org/10.1088/1361-6471/ab920b
35. P. L. Kerr, K. W. Kemper, P. V. Green, K. Mohajeri, E. G. Myers et al., Phys. Rev. C **54**, ID 1267 (1996). https://doi.org/10.1103/PhysRevC.54.1267
36. A. K. Basak, A. C. Merchant, M. Freer, M. S. Islam, R. A. Ramon et al., Euro phys. Lett. **138**, 44002 (2022). https://doi.org/10.1209/0295-5075/ac6c48
37. M. S. Islam, R. A. Ramon, M. M. Rahman, M. S. Islam, M. M. B. Azad et al., J. Phys. G, **48**, 125108 (2021). https://doi.org/10.1088/1361-6471/ac2fb0
38. M. A. Nagarajan, C. C. Mahaux, and G. R. Satchler, Phys. Rev. Lett. **54**, ID 1136 (1985). https://doi.org/10.1103/PhysRevLett.54.1136
39. M. E. Brandan and G. R. Satchler, Phys. Rep. **285**, 145 (1997). https://doi.org/10.1016/S0370-1573(96)00048-8
40. H. Esbensen, Phys. Rev. C, **77**, ID 054608 (2008). https://doi.org/10.1103/PhysRevC.77.054608

41. Ş. Mişicu and H. Esbensen, Phys. Rev. Lett. **96**, ID 112701 (2006). https://doi.org/10.1103/PhysRevLett.96.112701
42. A. K. Basak, P. K. Roy, S. Hossain, M. N. A. Abdullah, A. S. B. Tariq et al., Phys. Lett. B **692**, 47 (2010). https://doi.org/10.1016/j.physletb.2010.07.011